SANDIA REPORT

SAND2003-4551
Unlimited Release
Printed December 2003

Recyclable Transmission Line Concept for Z-Pinch Driven Inertial Fusion Energy

Stephen A. Slutz, Roger A. Vesey, Craig L. Olson, Kyle Cochrane, John S. De Groot and Per Peterson

Prepared by
Sandia National Laboratories
Albuquerque, New Mexico 87185 and Livermore, California 94550

Sandia is a multiprogram laboratory operated by Sandia Corporation,
a Lockheed Martin Company, for the United States Department of Energy's
National Nuclear Security Administration under Contract DE-AC04-94AL85000.

Issued by Sandia National Laboratories, operated for the United States Department of Energy by Sandia Corporation.

Available to DOE and DOE contractors from
U.S. Department of Energy
Office of Scientific and Technical Information
P.O. Box 62
Oak Ridge, TN 37831

Telephone: (865)576-8401
Facsimile: (865)576-5728
E-Mail: reports@adonis.osti.gov
Online ordering: http://www.doe.gov/bridge

Available to the public from
U.S. Department of Commerce
National Technical Information Service
5285 Port Royal Rd
Springfield, VA 22161

Telephone: (800)553-6847
Facsimile: (703)605-6900
E-Mail: orders@ntis.fedworld.gov
Online order: http://www.ntis.gov/help/ordermethods.asp?loc=7-4-0#online

SAND2003-4551
Unlimited Release
Printed December 2003

Recyclable Transmission Line Concept for Z-Pinch Driven Inertial Fusion Energy

Stephen A. Slutz and Roger A. Vesey
Target and Z-Pinch Theory Department

Craig L. Olson
Pulsed Power Science Center

Sandia National Laboratories
P. O. Box 5800
Albuquerque, NM 87185-1186

Kyle Cochrane
Ktech Corporation
1300 Eubank SE
Albuquerque, NM 87106-4265

J. S. De Groot
University of California, Davis
Davis, CA 95616

Per Peterson
University of California, Berkeley
Berkeley, CA 94720

Abstract

Recyclable transmission lines (RTL)s are being studied as a means to repetitively drive z pinches to generate fusion energy. We have shown previously that the RTL mass can be quite modest [S.A. Slutz, C.L. Olson, and Per Peterson, Phys. Plasmas, 429, 2003] Minimizing the RTL mass reduces recycling costs and the impulse delivered to the first wall of a fusion chamber. Despite this reduction in mass, a few seconds will be needed to reload an RTL after each subsequent shot. This is in comparison to other inertial fusion approaches that expect to fire up to ten capsules per second. Thus a larger fusion yield is needed to compensate for the slower repetition rate in a z-pinch driven fusion reactor. We present preliminary designs of z-pinch driven fusion capsules that provide an adequate yield of 1-4 GJ. We also present numerical simulations of the effect of these fairly large fusion yields on the RTL and the first wall of the reactor chamber. These simulations were performed with and without a neutron absorbing blanket surrounding the fusion explosion. We find that the RTL will be fully vaporized out to a radius of about 3 meters assuming normal incidence. However, at large enough radius the RTL will remain in either the liquid

or solid state and this portion of the RTL could fragment and become schrapnel. We show that a dynamic fragmentation theory can be used to estimate the size of these fragmented particles. We discuss how proper design of the RTL can allow this schrapnel to be directed away from the sensitive mechanical parts of the reactor chamber.

acknowledgments

We gratefully acknowledge the interest and support of Thomas Mehlhorn, Jeff Quintenz, Keith Matzen, and Dillon McDaniel. This work was performed under an LDRD.

Contents

Figures

I. Introduction

Z pinch physics has developed rapidly in the last few years. Nearly 2 MJ of thermal x-rays have been generated by this approach[1] with an overall efficiency greater than 15%, and much higher efficiencies should be possible with pulse power machines optimized for efficiency. Z-pinch generated thermal x-rays have been used to drive hohlraums[2] to temperatures greater than 200 eV, which were used to drive fusion capsules. One inertial fusion scenario[3] is to use two Z pinches to drive a central hohlraum containing a fusion capsule. Since Z-pinch implosions are subject to the Rayleigh-Taylor instability, this approach has the advantage of separating the nonuniformly emitting Z-pinch implosion from the inertial fusion capsule, but at the price of relatively low efficiency. Calculations[3] indicate that high yields (~400 MJ) could be obtained with 16 MJ of x-ray energy provided by two pinches driven with approximately 60 MA of current each. An alternate scheme[4] could provide much higher efficiency and thus lower the driver energy. In this "dynamic hohlraum" approach, a Z-pinch plasma is imploded onto a "convertor," which surrounds the capsule. Numerical simulations[5] indicate that a single pinch with 12 MJ of kinetic energy (55 MA) could drive a 500 MJ yield capsule, using this approach. Recent experiments indicate that the radiation generated within this convertor is relatively unaffected by the Rayleigh-Taylor instability[6] indicating that this higher efficiency approach may indeed be feasible.

Pulse power machines are robust and inexpensive when compared to other approaches for generating high energy densities, such as lasers or heavy ion beams, and the capability to operate reliably at high repetition rates has been demonstrated at small scale[7]. Thus pulsed power driven Z pinches could be an attractive approach to inertial fusion energy. However, a z-pinch driven fusion explosion will destroy a portion of the transmission line that delivers the electrical power to the z-pinch. On the present Z machine, these electrodes are constructed from ten tons of stainless steel. The cost of repairing the transmission line would outweigh the value of the energy created by the fusion explosion. Thus, up until recently, it has been assumed that this technology is limited to single-shot experiments.

Various means of providing standoff for z-pinch have been suggested. The most promising concept is the Recyclable Transmission Line (RTL), which emerged at a workshop[8] at Sandia National Laboratories and was developed further at the Snowmass[9] workshop on Fusion Energy. The idea is to construct the final portion of the transmission lines out of material that can be recycled inexpensively. The RTL concept is depicted schematically in Fig. 1.

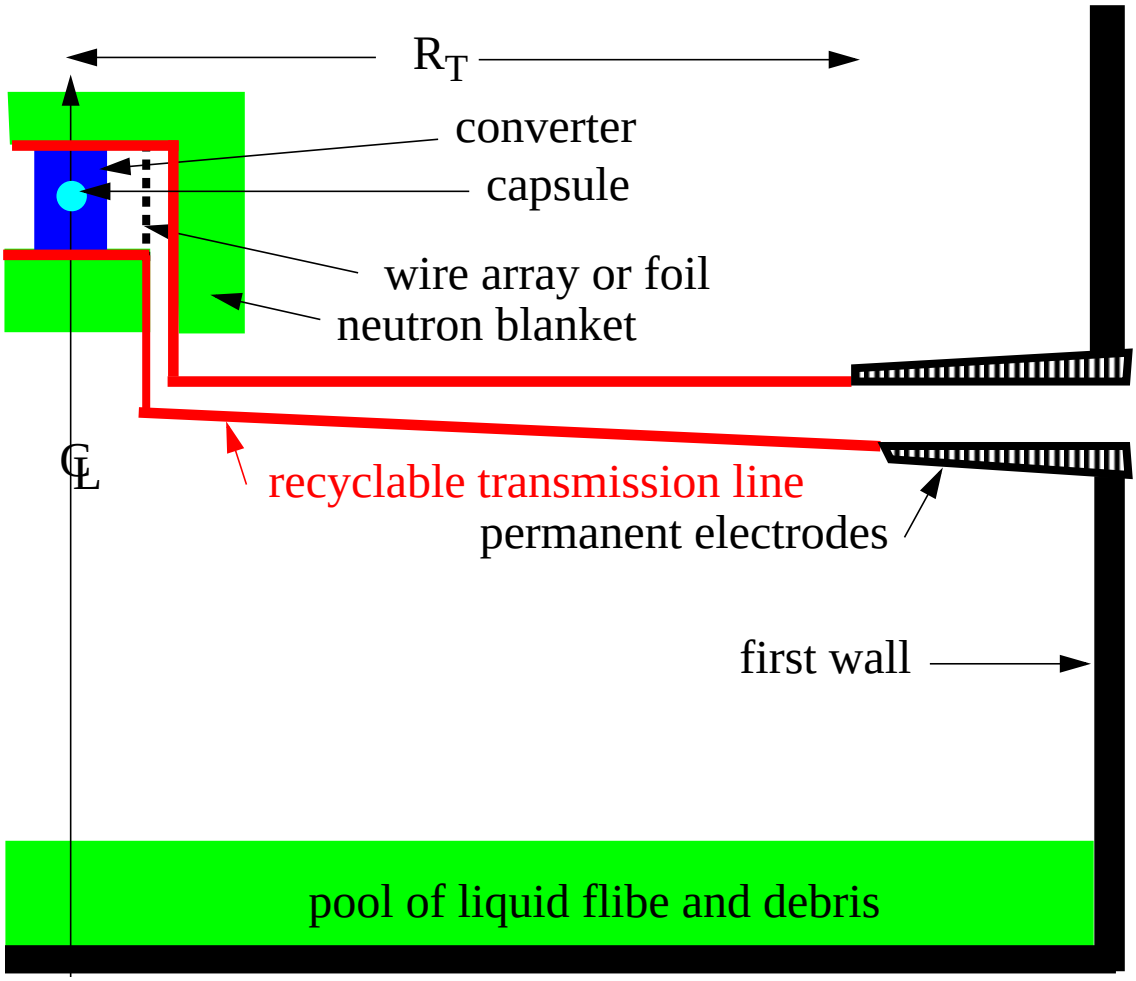

Fig. 1 Schematic of a Recyclable Transmission Line in a fusion chamber

The recyclable portion of the transmission line is shown in red. These RTLs could be formed inexpensively by casting of appropriate materials such as the reactor coolant flibe (a binary salt mixture of BeF_2 and LiF). However, solid flibe is an insulator so a coating of conducting material will be required in the inside surfaces of such an RTL. We have previ-

ously performed power flow tests, which indicated that either tin or aluminum could be used for this purpose[10]. Recent analysis suggest that the entire RTL could be constructed from an alloy of iron/carbon/tungsten. The components of this alloy are inert and immiscible in flibe, and will form a solid precipitate that can be recovered mechanically from the molten flibe by filtering and centrifugation processes. Activation products from these materials have relatively short half lives, so no long-lived radioactive waste would be generated. By maintaining carbon and tungsten concentrations around 1-2% by weight, the iron maintains the properties of steel and can be formed using the same processes used for fabricating sheet-metal components of automobiles, although remote fabrication will be required due to the activity from short-lived activation products.

Note that fluorine bearing materials such as flibe or LiH are common to fusion reactor design and serve two purposes. First, the lithium will absorb neutrons from the DT fusion reaction. This will produce the tritium needed for subsequent capsules and also protect the first wall from neutron damage. Second, this material will reduce the pressure generated at the first wall by the fusion explosion and thus reduces the standoff distance that is required to avoid damage. Ion beam driven inertial fusion schemes introduce this material as liquid waterfalls. The RTL concept allows these neutron blanket materials to be inserted as a solid very close to the fusion explosion as shown schematically in Fig. 1. Note that placing the neutron blanket close to the fusion explosion minimizes that amount of blanket material that is required to adequately protect the first wall from the neutrons.

The fusion yield must be large enough to compensate for the cost of recycling each RTL. We have estimated that a yield of 1 to 4 GJ should be sufficient. This is significantly larger than the yields of capsules designed for laser or ion beam fusion, which are about 150-700 MJ. We show in section II that both the double pinch and the dynamic hohlraum approach the z-pinch driven fusion can be scaled up to yields greater than a GJ but large currents (~ 100 MA) may be required.

In a previous report[11], we investigated the option of using low mass transmission lines (LMTLs) as a means of reducing the cost of recycling. The minimum transmission line mass is given approximately by the simple expression

$$M_{TOT} = 2\pi\Gamma_n R_T^2, \quad (1)$$

where R_T is the outer radius of the RTL (~ 3 m) and Γ_n is the minimum electrode areal density required for efficient power transport. We found that a carbon steel electrode with a thickness of 100 μm ($\Gamma_n = 0.8$ kg/cm^2) would efficiently transport up to 100 MA of current for a distance of several meters to a z pinch. This corresponds to an RTL mass of about 45 kg. Although this is drastically smaller than the present transmission line on the Z machine (~10 tons), it is much more mass than contained in the inertial fusion pellet (< 1 g) and will thus have a large effect on the impulse delivered to the first wall and the pulsed power driver. However, it should be noted that a neutron blanket capable of protecting the first wall will have a mass larger than the RTL.

It is our intent to minimize damage to sensitive components of the pulsed power driver by designing the RTL so that debris from the explosion will be directed away from the sensitive permanent electrodes. One possible scenario is to place the fusion capsule above an essentially disk shaped RTL so that the explosion will drive the debris downward into a pool of liquid flibe at the bottom of the reactor chamber as shown in Fig. 1. We are developing the capability to simulate the effect of the fusion explosion on the RTL and the reactor chamber. Ultimately these simulations will be 2D, but considerable information can be obtained with a series of 1D simulations. These simulations are presented in section III. A theory of dynamic fragmentation is outlined in section IV and an equation is developed to estimate the size of schrapnel fragments at radii large enough so that the RTL is not fully vaporized. A discussion of the implication of these results is presented in section V.

II. High Yield Z-pinch Driven Fusion Capsule for Energy

A promising inertial fusion scenario is to use to use two z pinches[3] to drive an external hohlraum containing a fusion capsule. The wire arrays stagnate and generate x-rays which first fill the primary hohlraums shown in Fig. 2. The x-rays, which are thermalized in these primary hohlraums, then flow into the secondary hohlraum. The calculated radiation temperature at the capsule is shown in Fig. 3 for the case of 16 MJ radiated by the two pinches.

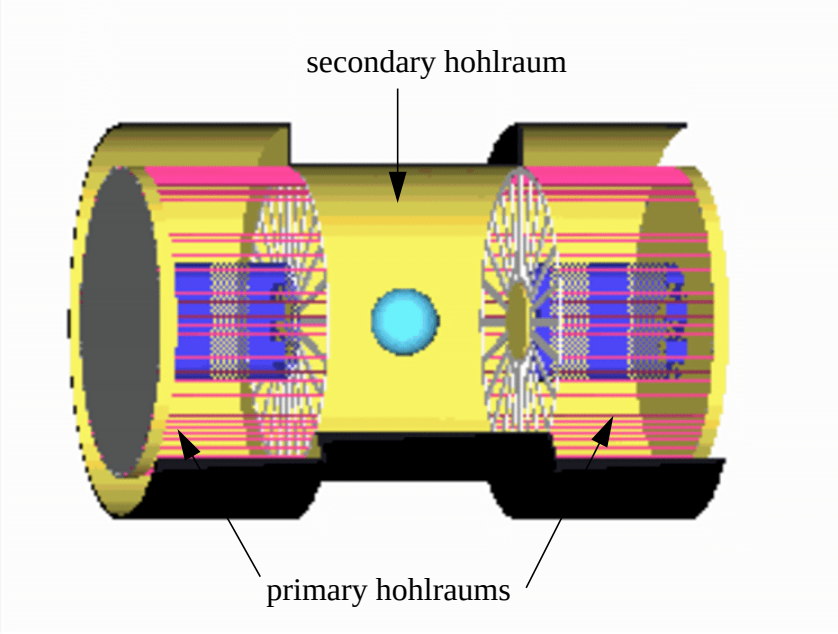

Fig. 2 Schematic of a double pinch driven fusion capsule

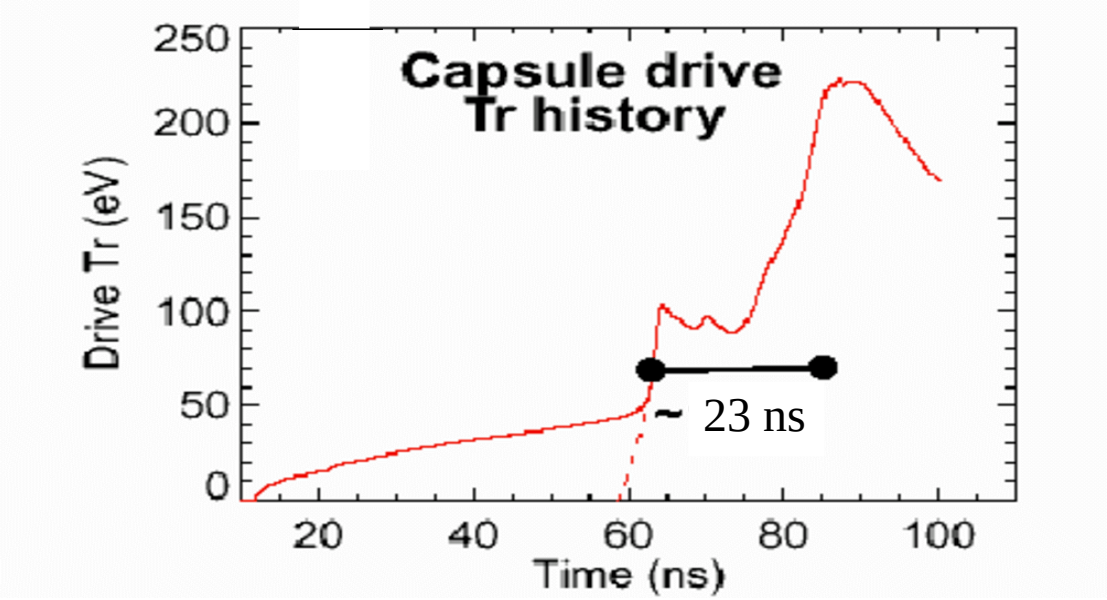

Fig. 3 Radiation temperature in the primary hohlraum

The details of the capsule are shown in Fig. 4. Simulations indicate the capsule produces a fusion yield of 400 MJ when driven by radiation temperature shown in Fig. 3.

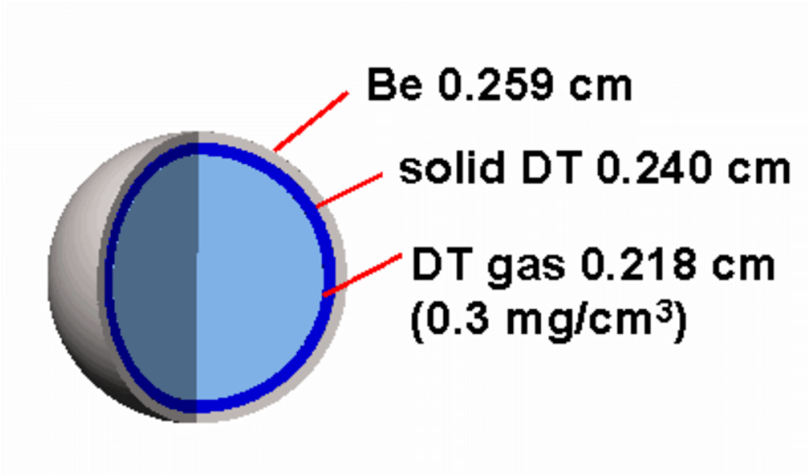

Fig. 4 400 MJ Double pinch capsule

We have revisited the design of the capsule. Using 1-D Lasnex simulations[12] we found that increasing the fuel thickness and capsule size substantially increases the yield up to a value of 1.2 GJ. The capsule dimensions are shown in Fig. 5.

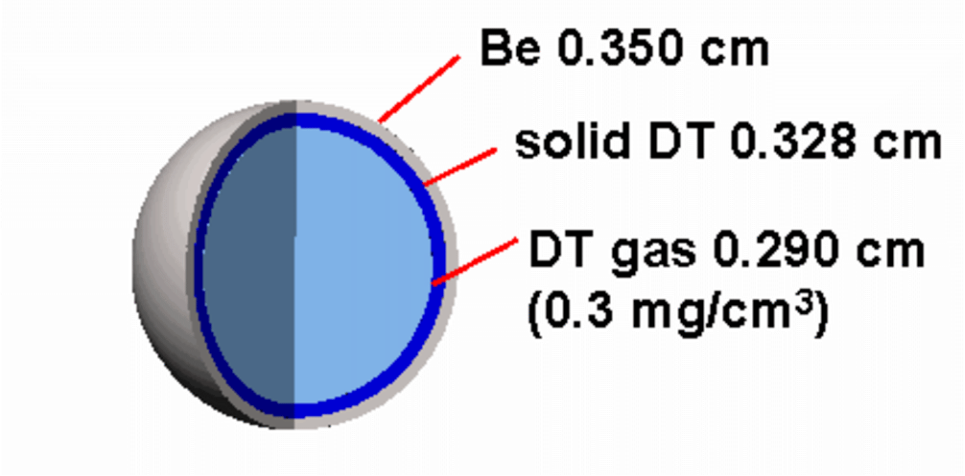

Fig. 5 Modified capsule parameters with a yield of 1.2 GJ

This capsule requires a somewhat different radiation temperature pulse shape due to the larger dimensions. The largest difference is the increased length of the radiation foot which is 29 ns as compared to 23 ns required for the smaller capsule. The radiation temperature is shown in Fig. 6.

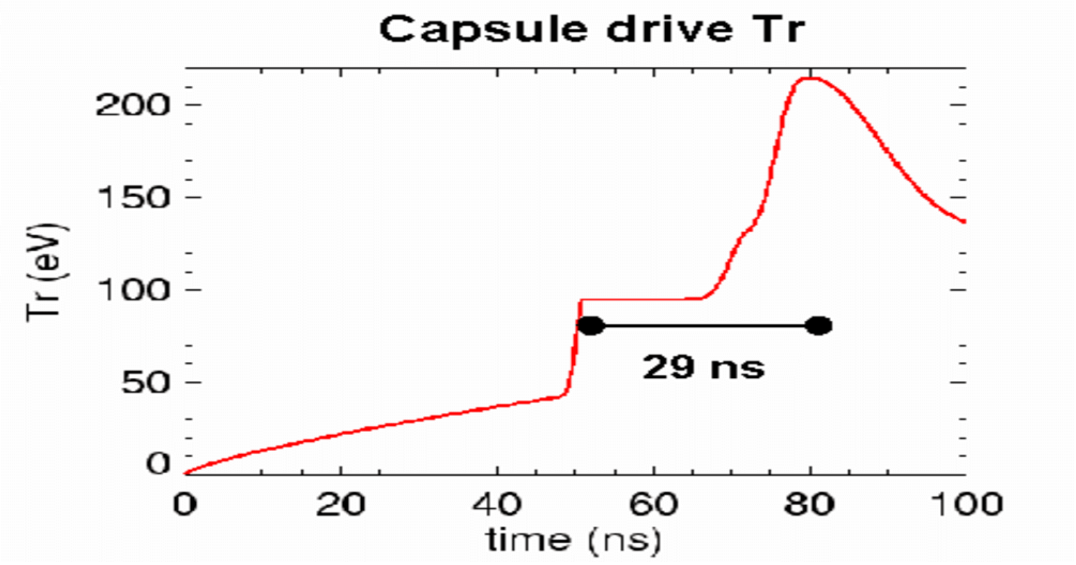

Fig. 6 Radiation temperature profile used to drive the modified capsule

In the double pinch approach a large fraction of the x-ray energy is absorbed by the hohlraum walls. This reduces the energy coupled to the capsule. The dynamic hohlraum is a more efficient approach to generating thermal radiation from z pinches. The dynamic hohlraum generates intense thermal radiation by driving a z-pinch plasma in a ‘convertor’, which is typically made of a low density material such as a plastic foam. A capsule can be located within the convertor as depicted in Fig. 7.

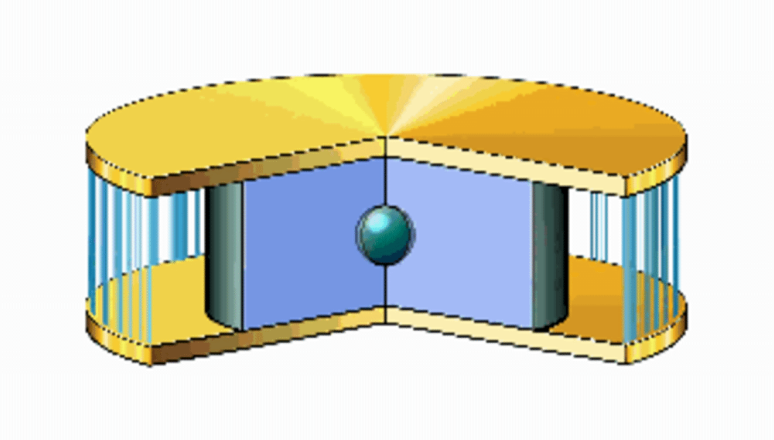

Fig. 7 Schematic of a dynamic hohlraum

The z-pinch plasma can be generated from a wire array or a solid liner. The implosion velocity of the z-pinch must be sufficiently high (> 20 cm/μs) to efficiently generate radiation. To obtain these velocities the z-pinch must be low mass (few 10s of mg/cm). Thus wire arrays have been the most successful since it is difficult to construct low mass liners without wrinkles, which seed the Magneto-Rayleigh-Taylor (MRT) instability. The mass of the z pinch can be increased with larger drive currents but the optimum initial wire radius also increases so wires may still be required for high yield designs.

When the z-pinch plasma strikes the convertor, a shock wave is formed, which propagates inward into the convertor. This shock wave heats the convertor material, which then emits radiation. A material of low opacity (typically a plastic foam) is chosen for the convertor so that radiation can easily flow inward to heat the ICF capsule The z-pinch plasma is composed of a material with high opacity (e.g. tungsten) to minimize the outward flow

of radiation and thus achieve maximal hohlraum radiation temperatures. The z-pinch plasma forms the walls of a hohlraum with much smaller dimensions than the walls of the double-ended z-pinch driven hohlraum and thus the dynamic hohlraum has less radiation loss and generates higher radiation temperatures.

Detailed numerical simulations[5] using Lasnex[12] indicate that a dynamic hohlraum could drive a moderately high yield capsule (500 MJ) with approximately 12 MJ of energy delivered to a single z pinch. This is roughly 75% of the energy that must be delivered to the double-ended z-pinch driven hohlraum. In addition, only two electrodes are required to drive the dynamic hohlraum, which is a significant advantage for energy applications. [Note that the double pinch can also be driven with one power feed (two electrodes), but with an energy penalty of roughly 15%.] A schematic of the dynamic hohlraum design is shown in Fig. 8.

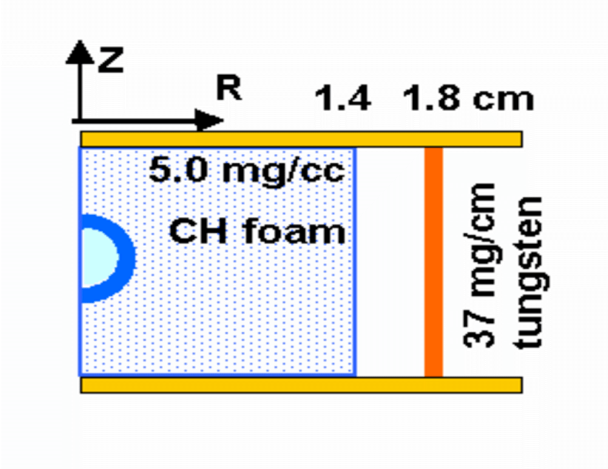

Fig. 8 A schematic of the 500 MJ dynamic hohlraum design

This hohlraum configuration resulted in a peak radiation temperature of 350 eV, which drove a capsule with parameters as shown in Fig. 9.

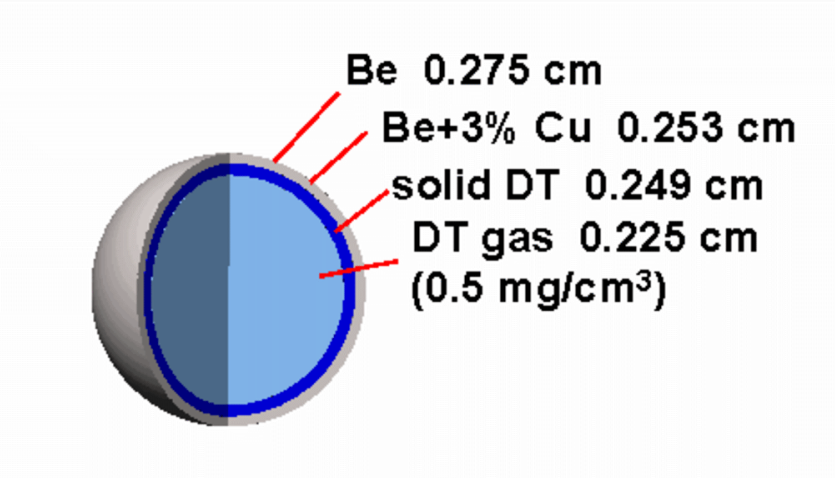

Fig. 9 Parameters of the 500 MJ dynamic hohlraum driven capsule

The capsule absorbs 2.3 MJ and yields 530 MJ. Multimode simulations indicate the capsule performance is insensitive to 1-2 μm of DT ice roughness. The fuel has 50% of its maximum kinetic energy at ignition, indicative of a robust design.

We have performed a preliminary scaling of this design to higher yields. The new dynamic hohlraum configuration is shown in Fig. 10.

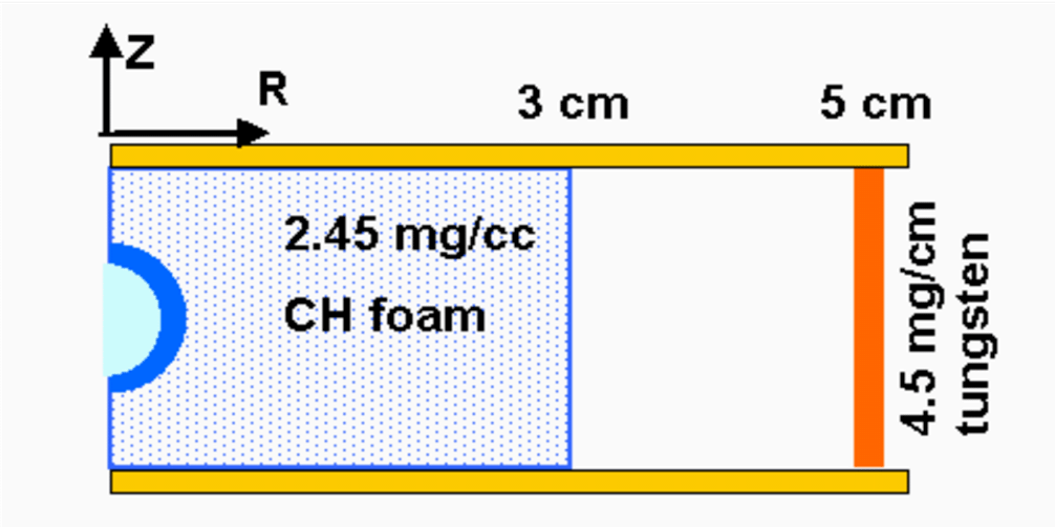

Fig. 10 A schematic of the 4 GJ dynamic hohlraum design

The convertor and wire array start at a larger radius to provide the appropriate pulse shape for the larger capsule. A Thevenin equivalent lumped circuit is used to model the pulsed power driving the current into the z pinch in Lasnex simulations of the dynamic hohlraum. The voltage waveform was scaled from the present Z machine. The peak voltage was increased by a factor of four to 20 MV and the risetime was increased by a factor of two to 200 ns. These circuit parameters produced a peak driving current of 95 MA. The calculations of the performance of this system are not fully integrated as in the previous design. Instead the radiation temperature profile is first determined with a 1-D cylindrical simulation of the wire array and the convertor. A cylindrical tube of the same radius as the capsule is imbedded in the convertor as a surrogate to the spherical capsule. This cylindrical capsule is important to the simulation results because the capsule ablation pressure helps to extract energy from the inward propagating shock wave. This phenomenon has been referred to as 'ablative standoff' in previous work[5]. The resulting radiation temperature profile is shown in Fig. 11.

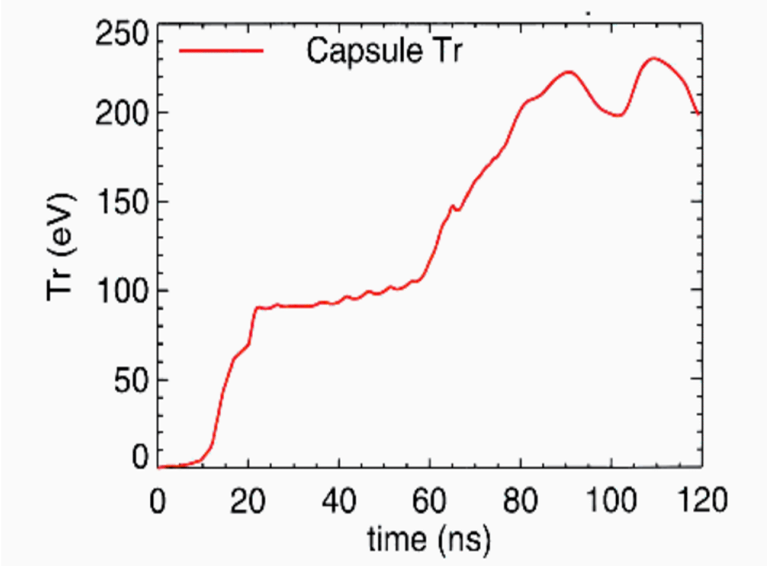

Fig. 11 The radiation temperature profile of a scaled up dynamic hohlraum

This radiation temperature profile was then used to drive a 1-D spherical capsule with the dimensions shown in Fig. 12.

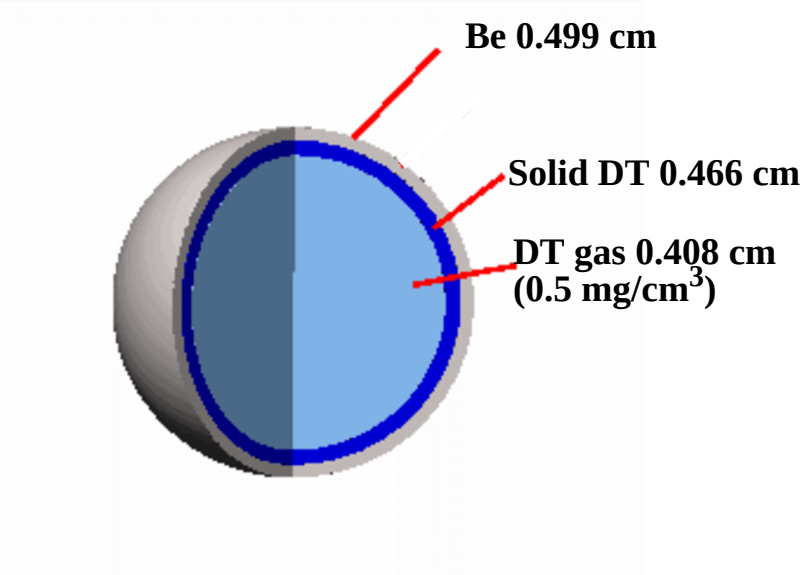

Fig. 12 The 4.6 GJ capsule parameters

The capsule absorbed 7.2 MJ of x-rays and produced a fusion yield of 4.6 GJ. The peak fuel ρr was 4.7 with a fuel burn up of 37%. The peak implosion velocity was 21 cm/μs and fuel kinetic energy was 38% of the maximum at the time of ignition. These parameters are indicative of a robust design. This capsule was not extensively optimized so higher performance should be possible. It should also be noted that the fast ignition concept[13] could substantially lower the drive requirements of such a large yield capsule. We plan to investigate this possibility and perform fully integrated 2-D simulations in the near future. Although more capsule design work is needed, we are confident that 100 MA should be sufficient to drive fusion capsules with yields of several gigajoules.

III. Fusion Explosion/RTL simulations

As we have discussed the RTL mass should be minimized to lower recycling costs. We found that an RTL mass of about 45 kg should efficiently transport 100 MA up to several meters[11], which is sufficient to drive a several gigajoule fusion capsule with standoff from

the permanent pulsed power components. Although this RTL mass is drastically smaller than the present transmission line on the Z machine (~10 tons), it is much more mass than contained in the inertial fusion pellet (< 1 g) and will thus have a large effect on the impulse delivered to the first wall and the pulsed power driver. At first this may seem to be a problem specific to the RTL approach to z-pinch driven fusion. However, both the ion beam and indirect drive laser driven fusion approach to inertial fusion energy typically assume liquid waterfalls of a lithium bearing compound to protect the chamber wall from 14 MeV neutron damage and breed tritium. The mass of this material is minimized if it is placed near the fusion capsule as shown in Fig. 1. Lithium-hydride will be the most effective material to stop neutrons and still breed tritium[14]. A mass of roughly 50 kg is needed to stop 90% of the neutrons, which is comparable the RTL mass. An even larger mass of about 150 kg is needed to produce as much tritium as would be used by a 50/50 DT capsule. Note that the fusion energy absorbed by the neutron blanket can be efficiently converted to electricity by the MHD process[14].

It is our intent to minimize damage to sensitive components of the pulsed power driver by designing the RTL so that solid and liquid debris from the explosion will be directed away from the sensitive permanent electrodes. One promising geometry is shown in Fig. 1. The capsule is placed above the disk shaped portion of the RTL so that the radiative ablation will drive the RTL downward. The blast from the explosion will also have a downward component and thus the debris will fall into a pool of liquid coolant (e.g. flibe) at the bottom of the reactor chamber. We are developing the capability to simulate the effect of the fusion explosions on the RTL and the reactor chamber. We start by simplifying the geometry of the RTL and the fusion capsule as shown in Fig. 13. Here the RTL is represented by a single disk (representing both electrodes) with the fusion capsule extended from this disk by a stalk (coaxial part of the RTL, see Fig. 1). The capsule is essentially surrounded by electrode material. For simplicity in our initial simulations we

lump all of the RTL material into a single spherical shell of 100 μm thick carbon steel with a radius of 8 cm.

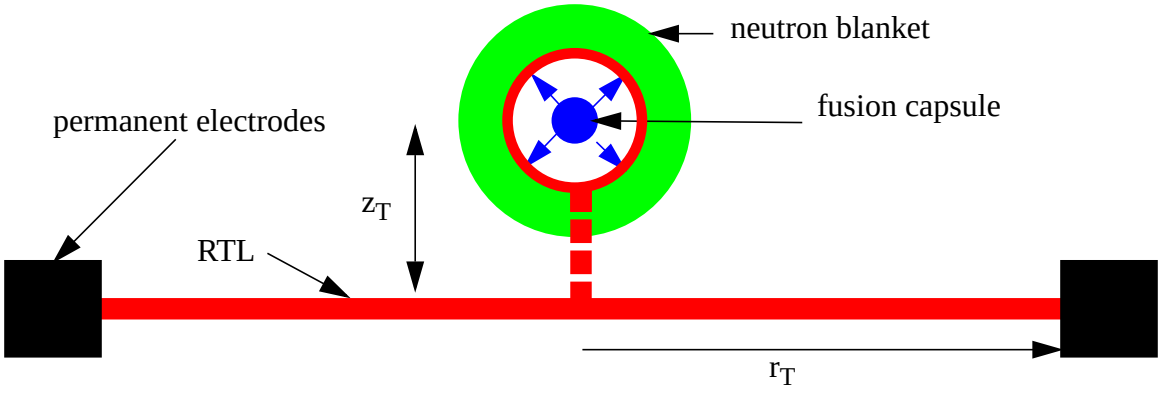

Fig. 13 Schematic of a simplified RTL

This can be further simplified by considering the 1D spherical geometry shown in Fig. 14, where we have essential bent the disk transmission line into a spherical shell. We can study the interaction of the fusion explosion at different points along the disk portion of the RTL by varying the radius of this outer RTL shell. We shall refer to the disk portion of the RTL as the DRTL, and the inner RTL shell as the IRTL

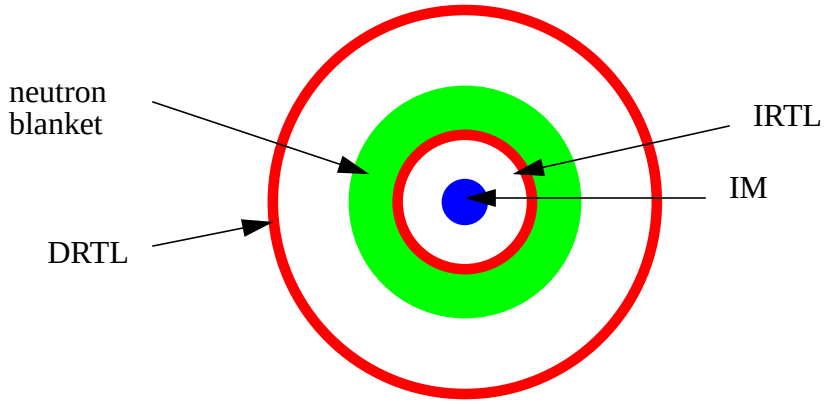

Fig. 14 Spherical geometry for studying RTL/fusion explosion interaction

At the time of ignition the z-pinch driven capsule will be surrounded by z-pinch wires and the convertor material. We lump these materials into a single region of mixed materials that we call the inner materials or IM. The IM consists of the capsule (~0.1 g CH and 0.03 g DT), the z-pinch wires (~ 0.13 g W) and convertor material (~ 0.2 g CH_2). We assume a fusion yield of 4 GJ of which only 20% will heat IM directly since the neutrons have a long range. The IM will heat up and expand, ultimately driving a shock wave into the IRTL. We have simulated this process using the Alegra[15] code. The radius of the outer IM surface and the inner and outer surfaces of the IRTL are plotted as a function of time in Fig. 15. The IRTL is heated by a shock wave produced by the expanding IM. It is also heated directly by x-rays emitted from the hot IM. Since iron has a high opacity these x-rays will essentially diffuse through the IRTL. This process is handled by multigroup diffusion in the Alegra code.

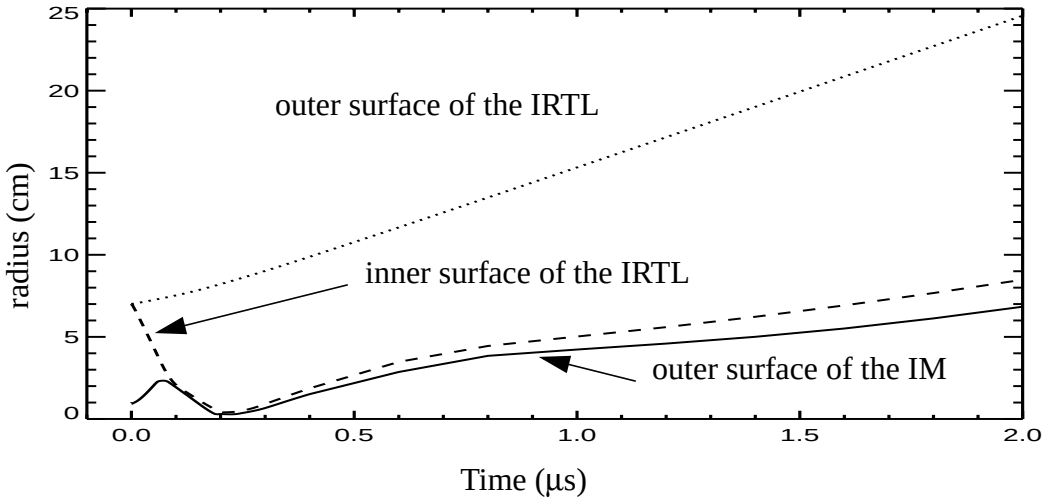

Fig. 15 Radial surface positions as a function of time

In response to shock and radiation heating mechanisms, the outer surface of the IRTL will become hot and emit x-rays. In the absence of a neutron blanket surrounding the shell these x-rays will radiate into the reactor chamber heating both the DRTL material and the

first wall. If the neutron blanket is present these x-rays will heat the blanket, which will also be heated by the neutrons. In this later case, the outer boundary of the blanket will radiate x-rays that will heat the DRTL and the chamber wall. We have performed simulations both with and without a neutron blanket. The neutron blanket was assumed to be flibe at a density of 2.3 g/cc and an outer radius of 11.4 cm. A separate Monte Carlo neutron transport calculation indicated that 70% of the 14 MeV neutrons will be stopped in this blanket. Note that considerably thicker neutron blankets (e.g. 25 cm radius LiH)[14] will be required to stop the low energy neutrons and generate as much tritium as used by the capsule. The Alegra simulations, which used multigroup diffusion, indicate that the spectrum emitted from either the IRTL shell or the outer boundary of the neutron blanket was essentially Planckian, except for an initial spike of high energy photons that can penetrate the IRTL. The radiation temperature at these surfaces is plotted in Fig. 16.

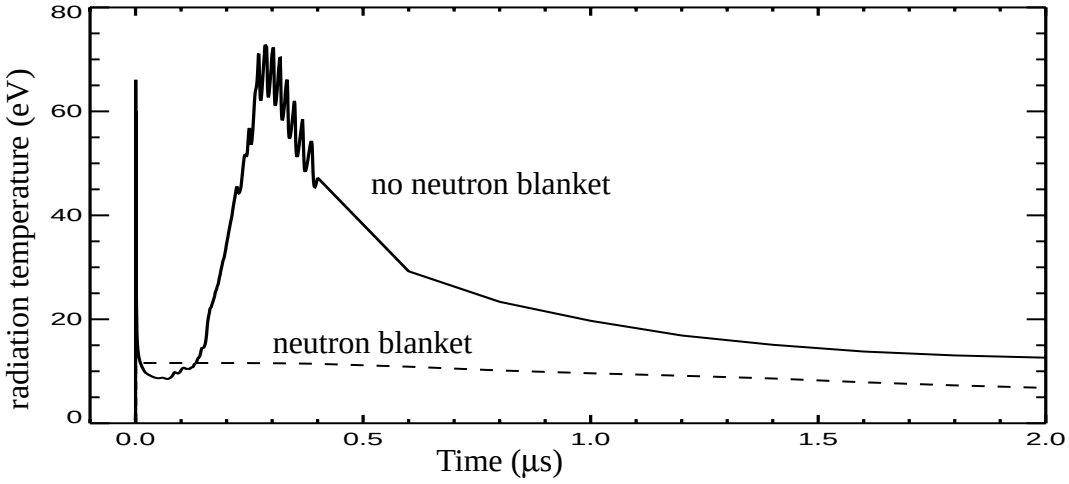

Fig. 16 Escaping radiation temperature plotted as a function of time

As can be seen even though a large fraction of the fusion yield is absorbed by the blanket, the radiation temperature is substantially reduced. This radiation will ablate surfaces within the reactor chamber until the material that is swept up in the explosion undergoes

impact. The positions of the outer boundary of the IRTL shell and the outer boundary of the neutron blanket are plotted as a function of time in Fig. 17.

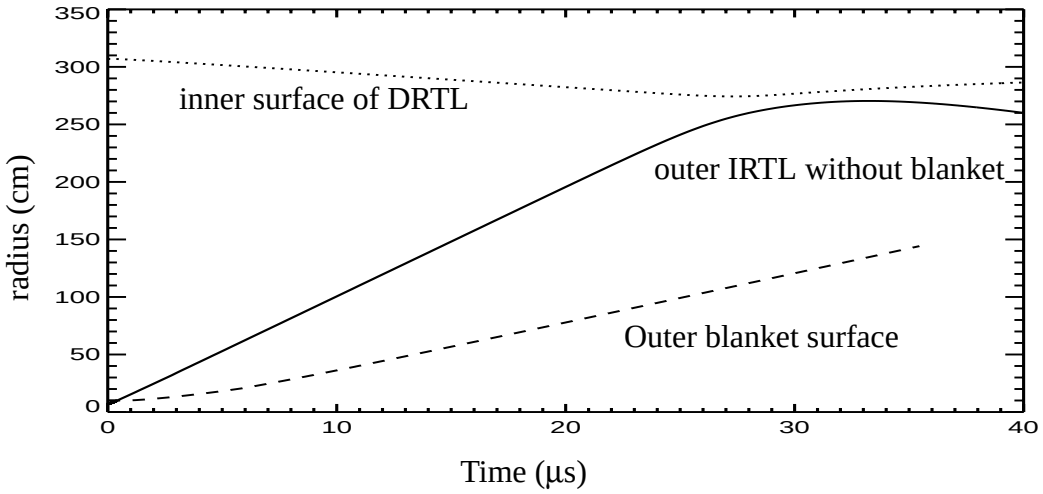

Fig. 17 Radial surface positions with and without a neutron blanket

The inner surface of the DRTL is shown for a simulation without a neutron blanket. This surface moves slowly inward in response to the x-rays that ablate the inner surface. The outer surface of the IRTL is also shown from this simulation. As can be seen, impact occurs at about 30 μs. The much slower moving outer surface of a neutron blanket from a different simulation is also shown for comparison. As expected the boundaries of either the IRTL or the neutron blanket asymptotically approach a constant velocity and thus it is easy to predict when this material will impact various surfaces within the chamber.

The simulations without a neutron blanket were performed with four different distances between the RTL shells (0.5, 1.0, 2.0, and 3.0) m. The average pressure on the inside surface of the DRTL for the simulations without the neutron blanket are plotted as a function of time in Fig. 18 and Fig. 19. The sharp initial spike in the pressure (Fig. 18) is due to the high energy component of the radiation spectrum the penetrates the IRTL. Impact of the IRTL plasma generates the pressure shown in Fig. 19. As can be seen the hydrodynamic pressure is as large as the pressure produced by radiative ablation, but extends over a longer period of time.

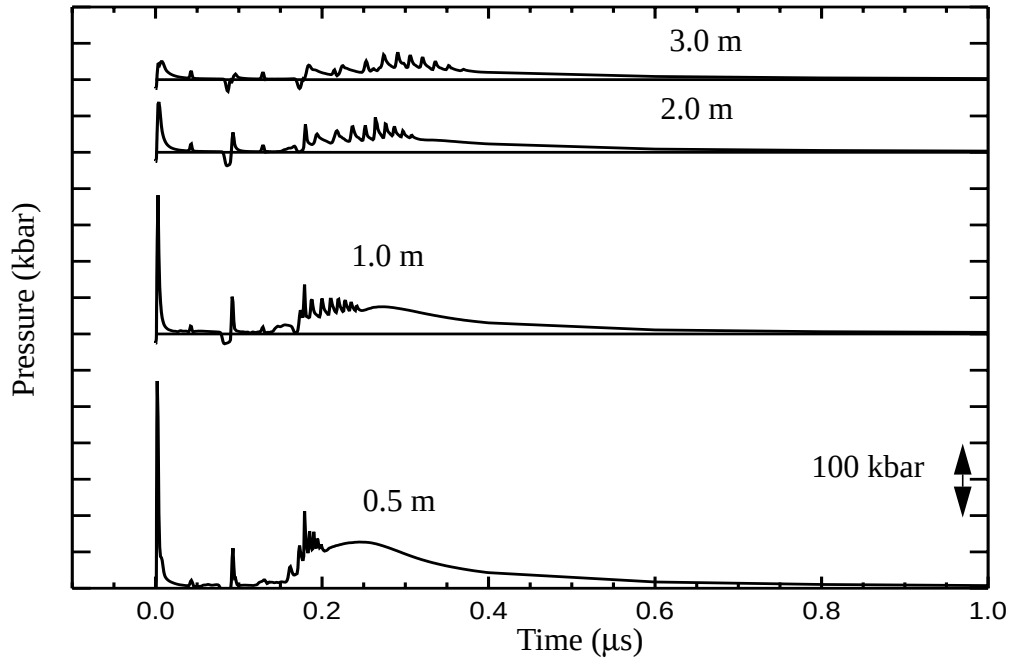

Fig. 18 Ablation pressure on the DRTL without a neutron blanket.

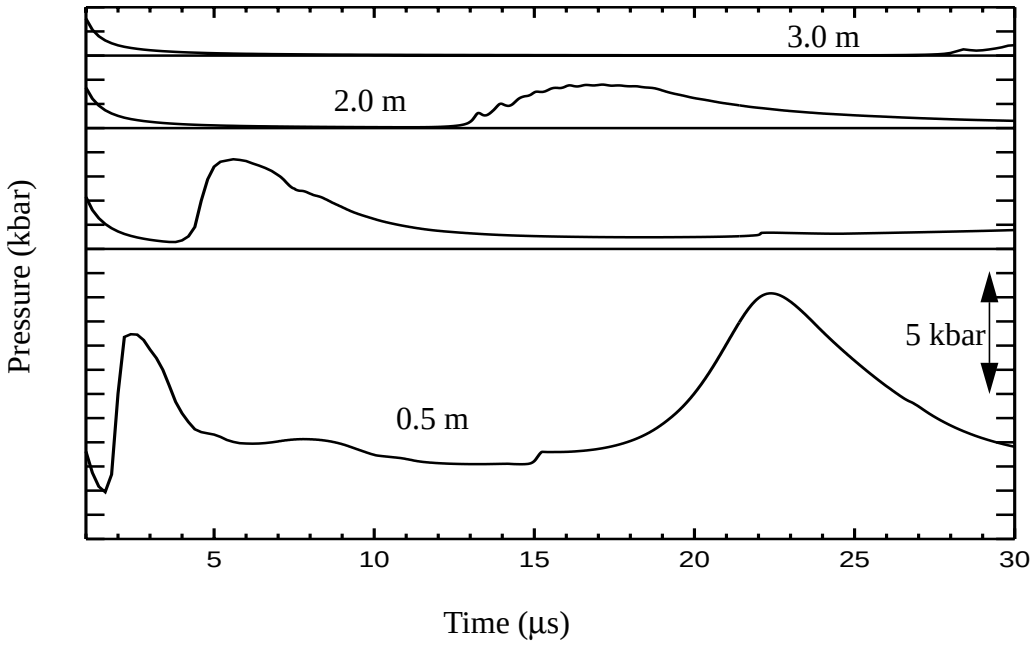

Fig. 19 Hydrodynamic pressure on the DRTL without a neutron blanket.

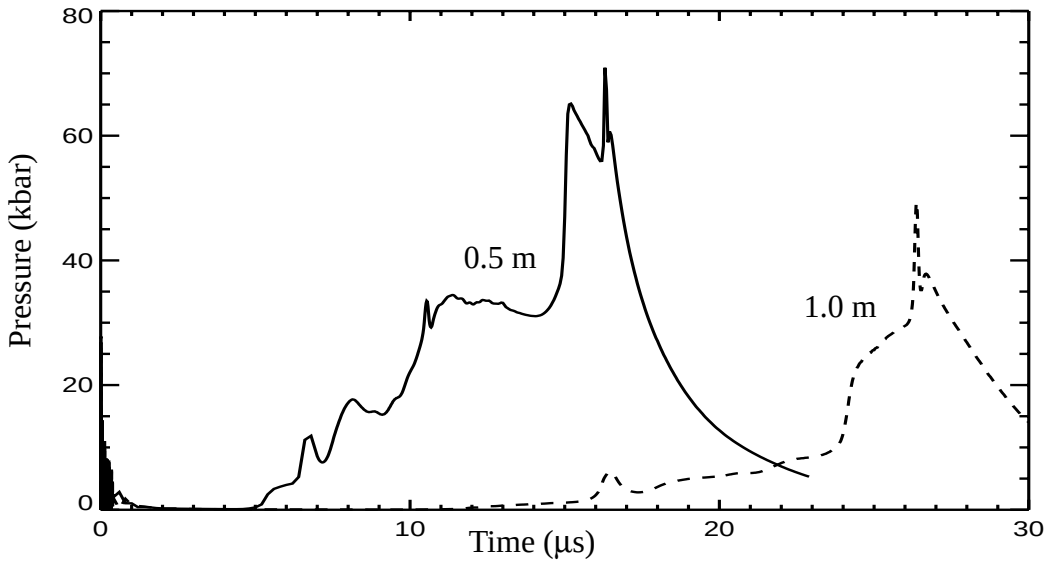

Fig. 20 Hydrodynamic pressure on the DRTL with a flibe neutron blanket

Alegra simulations were performed with DRTLs at 0.5 and 1.0 m from a flibe neutron blanket. The pressure generated on the inside of the DRTL for these simulations is shown in Fig. 20. In this case the only significant pressure is produced by the impact of the blanket with the DRTL. Note that the extra mass of the neutron blanket significantly increases the hydrodynamic pressure.

The impulse delivered to the DRTL or a first wall is found by integrating these curves. The results for simulations without a neutron blanket are plotted in Fig. 21 and the results with a neutron blanket are plotted in Fig. 22. The curves are labelled with the distance between the IRTL and the DRTL. As can be seen the neutron blanket significantly increases the impulse delivered.

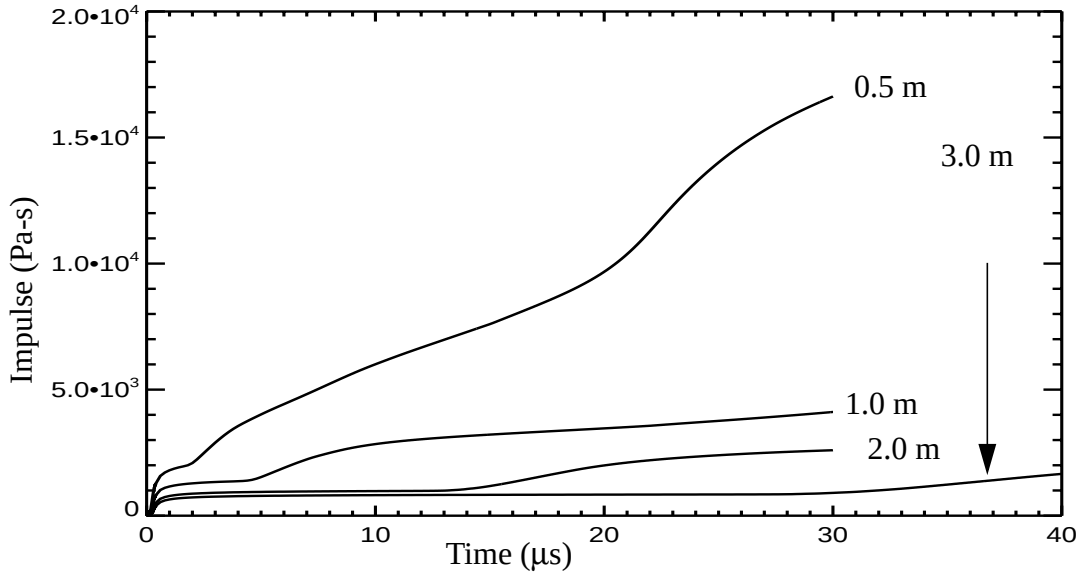

Fig. 21 Impulse delivered to the DMTL for no neutron blanket

.

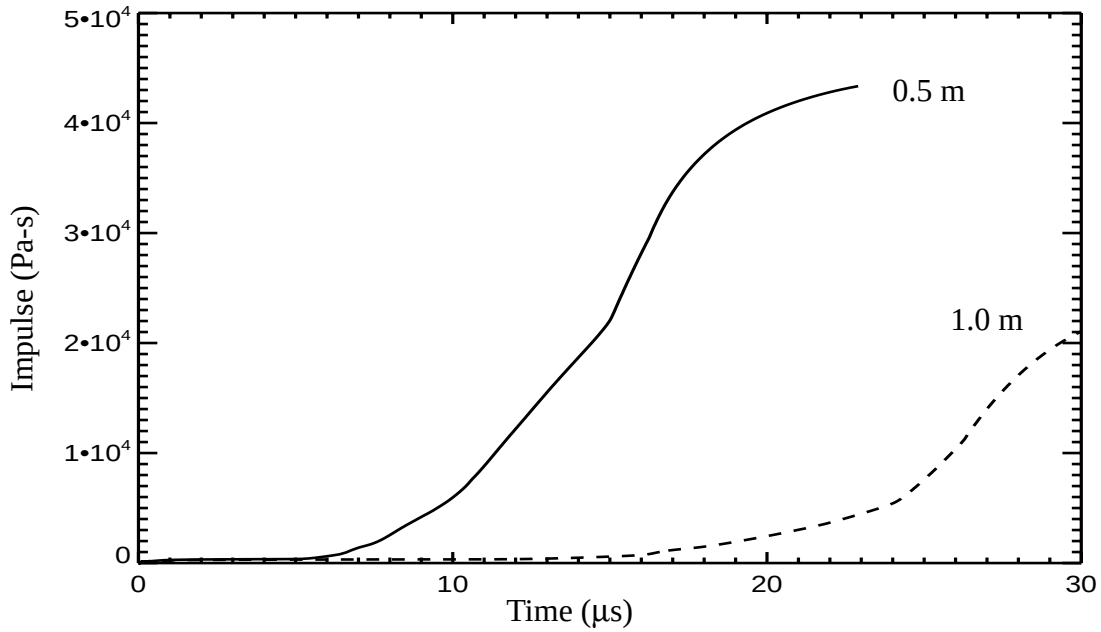

Fig. 22 Impulse delivered to the DMTL for a flibe neutron blanket

These curves can be used to determine the strength requirements of the vacuum chamber, a subject of future work. The DRTL is fully vaporized for all the cases that we ran. How-

ever, at radii larger than 3 meters the DRTL could remain solid or liquid. In this case we expect the pressure loading and release to fragment the RTL into schrapnel. These fragments could be harmful to the permanent transmission line or the reactor first wall. In the next section we present a theory of fragmentation that allows one to calculate the expected fragment size based on the rate of strain.

IV. Fragmentation of an RTL

The explosion of the fusion capsule, as calculated in the last section, can generate shock waves in the adjacent sections of the RTL. These shock waves are first generated by radiation ablation of the RTL by x-rays. An even stronger shock is then driven into the RTL by the material swept up by the explosion. Near the fusion explosion the shock will be strong enough to fully vaporize the RTL. However, at further distances the shock will leave the RTL in either a liquid or solid state. The pressure release at the edge of the RTL will generate shrapnel (liquid droplets or solid fragments), which can damage the sensitive components in the reaction chamber. A shock wave or the intense deposition of radiant energy on, and immediately within, the surface of a solid results in rapid heating of the material which is converted to thermal kinetic energy of the lattice and electronic structure[18]. The subsequent stress waves and decompression of the heated material can result in fragmentation of high-temperature solid, liquid and liquid-vapor matter.

An end-state theory of dynamic fragmentation based on balance of interfacial and dissipative energies resisting destabilization and breakup, and the energies of dynamic expansion, has been proposed[18,19]. The theory has been applied with some success to simple liquids, and to solids based on idealized models of toughness-controlled fracture (brittle spall) or plasticity-dominated hole growth and coalescence (ductile spall).

At temperatures above about 50% of the melt temperature, θ_m, the mobility of dislocations in most metals increases significantly, so that large levels of plasticity can be

accommodated with considerable ease. The precursor to fragmentation and growth is the growth and coalescence, and the local flow stress is the primary force resisting the cavity growth and breakup process. Within the energy-based theory of fragmentation the temperature and strain rate sensitivities of the flow stress at elevated temperature become critical material parameter descriptions governing the size of shrapnel.

For liquid metals, the surface energy is the principal material property governing the characteristic length scale of fragmentation. Surface tension (the property usually measured) and surface energy are related thermodynamically. Both are functions of temperature and approach zero as the temperature reaches the critical temperature. A broad base of data exist for liquid metals, and corresponding states relations for surface tension and surface energy allow for ready prediction of fragmentation in liquid metals at any temperature.

Under intense loading conditions the high entropy production in the shock process can be sufficient to cause the melting of metals when the dynamic pressure is released. The resulting fragments will be droplets. An energy based theory of spall and fragmentation in liquids has been developed[20]. This theory appears to correlate the relatively small base of dynamic fragmentation data available[18]. The principal mechanisms that inhibit fragmentation are the energy required to generate new surface area and viscous dissipation during the spall void growth and coalescence. The energy analysis predicts that surface energy dominates at lower fragmentation strain rates with a spall strength and average particle radius given by

$$P_{sv} = (6\rho^2 c_s^2 \gamma \dot{\xi})^{1/3} \quad \text{and} \quad r_s = \left(\frac{48\gamma}{\rho \dot{\xi}^2}\right)^{1/3}, \tag{2}$$

where ρ is the density, c_s is the sound speed $\dot{\xi} = \frac{1}{\rho}\frac{d\rho}{dt}$ is the strain rate, and γ is the surface energy per unit area of new fragment surface. At higher strain rates a transition to viscous-dissipation dominates fragmentation giving

$$P_{sv} = (2\rho c_s^2 \eta \dot{\xi})^{1/2} \text{ and } r_v = \left(\frac{8\eta}{\rho\dot{\xi}}\right)^{1/2}, \tag{3}$$

where η is the Newtonian viscosity. For liquid metals with η of the order of 10^{-3} Pa-s, the transition to viscosity-dominated fragmentation occurs at a strain rate of about 10^{12}/s.

The surface tension and the surface energy of a liquid both depend on the temperature. For liquid metals, the van der Waals relation[21],

$$\sigma = \sigma_0\left(1 - \frac{\theta}{\theta_c}\right)^n, \tag{4}$$

has been used successfully to describe the temperature dependence of the surface tension σ up to the critical temperature θ_c, where σ_0 and n are constants. The surface energy γ is thermodynamically related to the surface tension through the relation[18]

$$\gamma = \sigma - \theta\frac{d\sigma}{d\theta}. \tag{5}$$

Using Eq. (4) we obtain the expression

$$\gamma = \sigma_0\left(1 - \frac{\theta}{\theta_c}\right)^n\left(1 + \frac{n\theta}{\theta_c - \theta}\right). \tag{6}$$

The van der Waals constants σ_0 and n can, in principle, be determined from measurements of the surface tension and its first derivative at the melt temperature. Working with Eq. (4) and its first derivative, the relations

$$n = -(\theta_c - \theta_m)\frac{\sigma_m'}{\sigma_m} \text{ and } \sigma_0 = \sigma_m\left(1 - \frac{\sigma_m}{\sigma_c}\right)^{-n} \tag{7}$$

are obtained. The subscript m refers to properties evaluated at the melt temperature. The point is that we assume that fragmentation occurs at the melt temperature.

Substantial surface tension data exists for liquid metals[21]. However, data for the temperature derivative of the surface tension σ_m' are not known with sufficient accuracy to constrain n. A more successful approach[22] is based on a general observation relating the surface tension to the temperature decrement below the critical temperature,

$$\sigma\left(\frac{A}{\rho}\right)^{2/3} = k(\theta_c - \theta), \tag{8}$$

where A is the molecular weight and k is a constant. Using Eq. (8), one obtains

$$n = \frac{2}{3}\alpha_m(\theta_c - \theta_m) + 1, \tag{9}$$

where α_m is the coefficient of thermal expansion at the melt temperature. Values of n ranging from about 1.1 to 1.7 are calculated for liquid metals[18].

A promising candidate material for an RTL is iron. The characteristic parameters for iron are[18]; ρ = 7.0 g/cc, $\alpha_m = 1.2\times10^{-4}$ K^{-1}, θ_m = 1810 K, θ_c = 6330 K, σ_m = 1.9 N/m, σ_0 = 2.9 N/m, n = 1.34, and $c_s = 4.5\text{x}10^5$ cm/s.

Substituting these values into Eq. (6) we find the surface energy at the melt temperature is, γ_m = 2 J/m. Then using Eq. (2) we find the droplet size as a function of the strain rate,

$$r_s = \frac{2.7\times10^5}{\dot{\xi}^{2/3}}. \tag{10}$$

Thus the fragment size can be expected to increase with distance from the fusion explosion. In the last section simulations were performed to estimate the effect of a 4 GJ fusion explosion on the surrounding RTL. In all the cases we simulated the RTL is fully vaporized so no fragments could result. However, just to get a feeling for Eq. (10), consider the results for an RTL at radius of 50 cm and no neutron blanket. The shock breaks out of the back of the RTL about 10 μs after the explosion and the maximum strain rate is $1.2\text{x}10^7$,

sec^{-1}. From Eq. (10) we see that the average droplet diameter would be about 10 μm. The velocity of the droplets should correspond to the shock velocity, which is approximately $5x10^4$ cm/s. Such small fragments could be stopped easily in a liquid waterfall of flibe. However, larger, but slower fragments would be generated at larger radii. Ultimately we intend to simulate the RTL response to fusion explosions at varying distances and conditions (e.g. presence of a neutron blanket) and use Eq. (10) to estimate the spectrum of fragment sizes.

V. Summary

The RTL approach to repetitive z pinch driven fusion requires a substantial fusion yield to offset the cost of recycling. We have presented preliminary numerical designs of fusion capsules with yields of 1-4 GJ, which should be adequate for fusion energy applications.

The effect of the fusion explosion on the RTLs has been investigated numerically. We have performed 1-D simulations to estimate the radiation that will emanate from the fusion explosion and the effect of this radiation on portions of the RTL at various distances from the center of the explosion. We find that the presence of a neutron blanket around the explosion can significantly reduce the radiation. The RTL material within 3 meters of the explosion will be immediately vaporized assuming normal incidence. RTL material at sufficiently large radius or with a nonnormal incidence could possibly become schrapnel.

We present an end-state theory of dynamic fragmentation based on balance of interfacial and dissipative energies resisting destabilization and breakup, and the energies of dynamic expansion to calculate the size of the schrapnel particles. We plan to use this theory to estimate size of schrapnel particles. The fragments will be larger at distances further from the explosion. It should be possible to direct these fragments away from the sensitive permanent transmission line components by proper shaping of the RTL. As future work

we plan to perform full 2-D simulations of the fusion explosion and its effect on the RTL to demonstrate this.

References

1 R.B. Spielman, C. Deeney, and G.A. Chandler, Phys. Plas. 5, 2105 (1998).

2 S.A. Slutz, J.E. Bailey, G.A. Chandler et al. Phys. Plasmas, 5, 1875, (2003).

3 J. H. Hammer, M. Tabak, S. C. Wilks, J. D. Lindl, D. S. Bailey, P. W. Rambo, A. Toor, G. B. Zimmerman, Phys. Plasmas, 6, 2129, 1999.

4 J. H. Brownell, R. L. Bowers, Bull. Am Phys. Soc. 40, 1848 (1995)

5 J. Lash, G.A. Chandler, G. Cooper, M.S. Derzon, M.R. Douglas, D. Hebron, R.J. Leeper, M.K. Matzen, T.A. Mehlhorn, T.J. Nash, R.E. Olson, C.L.Ruiz, T.W.L. Sanford, S.A. Slutz, D.L. Peterson, and R.E. Chrien, "The Prospects for High Yield ICF with a Z-Pinch Driven Dynamic Hohlraum", Proceedings of Inertial Fusion Science and Applications 99, Bordeaux, FR, Sept. 1999, edited by C. Labaune, W.J. Hogan, K.A. Tanaka (Elsevier, Paris, 2000), Vol. I, p. 583

6 J.E. Bailey et al. Bull. Am. Phys. Soc. 43, 105, (2001); and J.E. Bailey, G.A. Chandler, S.A. Slutz et al. Phys. Rev. Lett, 89, 095004-1 (2002).

7 D. L. Johnson, K.W. Reed et al., 9th IEEE International Pulsed Power Conference, Ed. K. Prestwich and W. Maker, Albuquerque, NM, 1993

8 Spielman, R. B. 1999. *Z-Pinch Fusion for Energy Applications. SAND99-3155,* Sandia National Laboratories, Albuquerque, NM

9 *Proceedings of the 1999 Fusion Summer Study,* Snowmass CO. Editors R. Hawryluk., G. Logan, and M. Mauel; C. L. Olson, Comments on Plasma Phys. Controlled Fusion, Comments on Modern Physics, Vol. 2(2), p. 113 (2000).

10 C.L. Olson, S.A. Slutz, G.E. Rochau, M.S. Derzon, P.F. Peterson, J.S. DeGroot, G.A. Rochau, R.R. Peterson, SAND2001-1736, Sandia National Laboratories, Albuquerque, NM.

11 S.A. Slutz, C.L. Olson, and Per Peterson, Phys. Plasmas, 429, 2003.

12 G.B. Zimmermann and W.L. Kruer, Plasma Phys. Controlled Fusion 2, 51 (1975)

13 M. Tabak, J. Hammer, M.E. Glinsky, W.L. Kruer, S.C. Wilks, J. Woodworth, E.M. Campbell, M.D. Perry, and R.J. Mason, Phys. Plasmas 1, 1626 (1994).

14 B.G. Logan, Fusion Engineering and Design, 22, 151, (1993).

15 E.A. Boucheron, K.H. Brown, K.G. Budge et al. “ALEGRA: User Input and Physics Descriptions Version 4.0”, SAND 2001-1992, 2001.

16 S.A. Slutz, M.R. Douglas, J.S. Lash, R.A. Vesey, G.A. Chandler, T.J. Nash, and M.S. Derzon, Phys. Plas. 5, 1673

17 P.F. Peterson, C. Cole, A. Donelli, and D.R. Olander, First International Conference on Inertial Fusion Sciences and Applications, University Bordeaux, France, Sept. 12-17, 1999.

18 D. E. Grady,’High-Pressure Shock Compression of Solids II’ (Springer, 1996).

19 D.E. Grady, J. Applied Phys. 53, 322 (1982);

20 D.E. Grady, J. Mech. Phys. Solids 3, 353 (1988).

21 B. C. Allen, “The Surface Tension of Liquid Metals” article in “Liquid Metal Chemistry and Physics”, p 151 (1972)

22 Eotvos, R., Ann. Phys. Chem. 27, 448 (1886).

distribution

10 Prof. Per F. Peterson
Dept. of Nuclear Engineering
4111 Etcheverry
University of California
Berkeley, CA 94720-1730

2 Cornell University
Laboratory of Plasma Studies
Attn: D. A. Hammer
J. B. Greenly
369 Upson Hall
Ithaca, NY 14853

5 Lawrence Livermore National Laboratory
Attn: John Perkins L-637
J. Hammer L-018
John Lindl L-039
M. Tabak L-015
W.R. Meier L-641
P.O. Box 5511 7000 East Ave
Livermore, CA 94550

2 Imperial College
Attn; M. Haines
G. Chittenden
South Kensington, London
SW72BZ, United Kingdom

1 Institute fur Kernphysik
Attn: D. H. H. Hoffmann
Strahlungs-und Kernphysic
TU Darmstadt, Karolinenplatz
D 64289 Darmstadt, Germany

1 Universite Paris SUD
Attn: C. Deutch
Laboratoire de Physique des Gas et des Plasmas
BAT 210 LP CEP R-91405
Orsay, France

3 University of Nevada Reno
Attn: B. Bauer MS-220
Attn: T. Cowan MS-220
Attn; R.E. Siemon MS-220
Department of Physics, Reno, NV 89557

2 Los Alamos National Laboratories
Attn: D. Peterson X-PA
Attn; R. R. Peterson
Los Alamos, NM 87545

1 Lawrence Berkeley National Laboratory
Attn: B. G. Logan
1 Cyclotron Rd.
Berkeley, CA 94720

5 University of California Davis
Attn: J. DeGroot
Dept. of Applied Science
Rm 228 Walker Hall
Davis, CA 95616

1	MS-0323	1011	H. R. Westrich
1	MS-0151	16000	G. Yonas
1	MS-0736	6400	T. E. Blejwas
1	Ms-0865	1900	D. Cook
30	MS-1188	9500	C. Olson
1	MS-1190	1600	J. Quintenz
1	MS-1191	1670	M. Sweeney
1	MS-1181	1610	J. Asay
1	MS-1178	1630	D. Bloomquist
1	MS-1194	1640	D. McDaniel
1	MS-1194	1612	C. Deeney
1	MS-1194	1644	W. Stygar
1	MS-1191	1600	K. Matzen
1	MS-1193	1673	J. Porter
1	MS-1186	1674	T. Mehlhorn
1	MS-1196	1677	J. Bailey
1	MS-1193	1673	M. Cuneo
1	MS-1186	1674	M. P. Desjarlais
20	MS-1186	1674	S. Slutz
1	MS-1186	1674	R. Vesey
1	MS-1196	1677	R. Leeper
1	MS-1196	1677	G. Chandler
1	MS-1196	1677	R. E. Olson
1	MS-1196	1677	T. Sanford
1	MS-0748	6415	G. Rochau
1	MS-0748	6415	C. Morrow
1	MS-9018	8945-1	Central Technical Files
2	MS-0899	9616	Technical Library
1	MS-0323	1011	LDRD Office